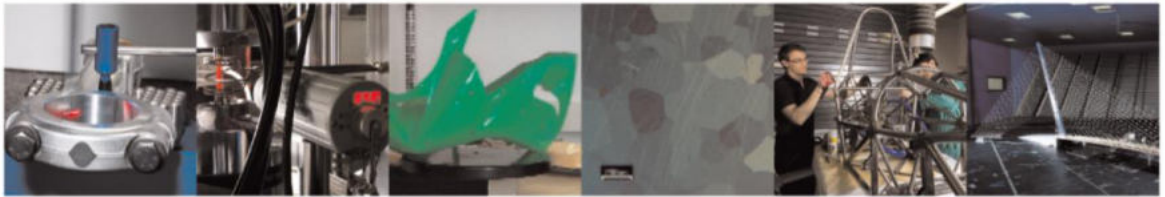




**POLITECNICO**  
MILANO 1863

DIPARTIMENTO DI MECCANICA



## Mill condition monitoring based on instantaneous identification of specific force coefficients under variable cutting conditions

Luca Bernini, Paolo Albertelli, Michele Monno

This is a post-peer-review, pre-copyedit version of an article published in Mechanical Systems and Signal Processing. The final authenticated version is available online at:

<http://dx.doi.org/10.1016/j.ymssp.2022.109820>

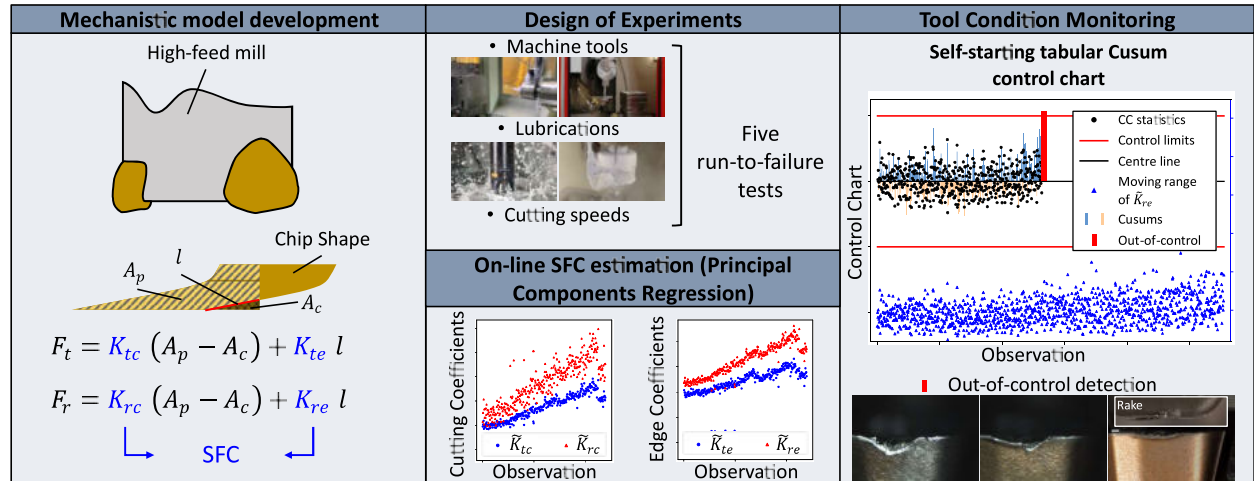
This content is provided under [CC BY-NC-ND 4.0](https://creativecommons.org/licenses/by-nc-nd/4.0/) license



## Graphical Abstract

### Mill condition monitoring based on instantaneous identification of specific force coefficients under variable cutting conditions

Luca Bernini, Paolo Albertelli, Michele Monno



## Highlights

### **Mill condition monitoring based on instantaneous identification of specific force coefficients under variable cutting conditions**

Luca Bernini, Paolo Albertelli, Michele Monno

- Double-phased high-feed cutters mechanistic model development.
- Specific Force Coefficients online estimation by Principal Component Regression.
- Self-starting control chart for unsupervised robust Tool Condition Monitoring.

# Mill condition monitoring based on instantaneous identification of specific force coefficients under variable cutting conditions

Luca Bernini<sup>a,b,\*</sup>, Paolo Albertelli<sup>a,b</sup> and Michele Monno<sup>a,b</sup>

<sup>a</sup>Department of Mechanical Engineering, Politecnico di Milano, via La Masa 1, Milan 20156, Lombardy, Italy

<sup>b</sup>MUSP Macchine Utensili Sistemi di Produzione, strada della Torre della Razza, Piacenza 29122, Emilia-Romagna, Italy

## ARTICLE INFO

### Keywords:

Tool condition monitoring  
Analytical model development  
Specific force coefficients  
Instantaneous forces identification  
High-feed mills  
Self-starting control charts

## ABSTRACT

Following the necessity of increased performance and availability requirements for manufacturing systems, research is becoming more and more attracted by monitoring solutions for cutting tools. In this paper, a robust unsupervised strategy for milling tool wear monitoring under variable process parameters and lubrication conditions is presented. The proposed method is completely unsupervised, thus not requiring any kind of training procedure, and is validated on different machine tools. The solution is based upon the online estimation of specific force coefficients (SFC) from instantaneous cutting forces in high-feed milling of  $Ti_6Al_4V$  workpiece. This avoids the need for continuously variable feed per tooth during cutting tests, necessitated for the application of reference literature approach. For this purpose, a novel high-feed mill mechanistic model was conceived and developed. Five run-to-failures were performed in different lubrication conditions - cryogenic and traditional lubrication - with different cutting speeds ( $50\text{m/min}$ ,  $70\text{m/min}$  and  $125\text{m/min}$ ) on two different machine tools. Principal Component Regression was introduced in order to deal with the variability of the estimated coefficients. Self-starting tabular cusum control charts were implemented and demonstrated high accuracy and reliability in the prediction of notch wear phenomena as well as chipping of tool cutting edges for all the cases considered. The solution detected an out-of-control conditions ranging from  $166\mu\text{m}$  to  $499\mu\text{m}$  of maximum flank wear for the analysed tests. The mean prediction error with respect to the  $600\mu\text{m}$  threshold is of  $-45\%$  with a peak of  $-72\%$ , whereas reference literature algorithms reach  $-57\%$  and  $-66\%$ , respectively. A sensitivity analysis of control chart threshold was performed with reference to the maximum flank wear at the detection point. In a supervised scenario, the threshold can be increased to obtain a less conservative approach: for instance, a mean prediction error of  $-41\%$  was reached by doubling the threshold.

## 1. Introduction

The complexity of manufacturing systems has been increasing in order to accomplish the high reliability and safety that industry demands (Peng, Dong and Zuo (2010)). Furthermore, plants require high-quality machining and high-quality tools for automation. The development of condition monitoring solutions for machine tool components and processes became means to reach these goals (Albertelli, Goletti, Torta, Salehi and Monno (2016)). Thus, research has been focusing on the study of cutting tool condition monitoring (TCM) and prognostics approaches (Baur, Albertelli and Monno (2020)). This was related to the fact that the cutting tool provides large cost saving possibilities; up to 40% could be achieved through the monitoring of its health (Stavropoulos, Papacharalampopoulos, Vasiliadis and Chrysosolouris (2016)). Furthermore, about 20% of the downtimes of machine tools was attributed to tool failures, resulting in reduced productivity and economic losses (Kurada and Bradley (1997); Zhang, Wang, Li and Lu (2021)). TCM strategies represent also transition means towards sustainable manufacturing. Tool wear assessment and prediction can be an important resource to feed process parameter optimization algorithms (Kuntoğlu, Aslan, Pimenov, Usca, Salur, Gupta, Mikolajczyk, Giasin, Kapłonek and Sharma (2020a); Kuntoğlu, Aslan, Sağlam, Pimenov, Giasin and Mikolajczyk (2020b); Aslan (2020); Zhang, Pan, Ma and Zhao (2022b)). In fact, a proper optimization of cutting parameters during the cut can extend their remaining useful life, reducing the amount of waste materials (Zhou, Guo and Sun (2021); Zhang, Yu, Xu and Zhao (2022c)).

Basically, two strategies can be adopted for TCM, either based on direct measurements or indirect ones: the first one, where the assessment of the tool is carried out by measurements of a wear characteristics (e.g. flank wear), whereas the

\*Corresponding author

✉ luca1.bernini@polimi.it (L. Bernini); paolo.albertelli@polimi.it (P. Albertelli); michele.monno@polimi.it (M. Monno)  
ORCID(s): 0000-0002-7064-7518 (L. Bernini); 0000-0001-5098-0420 (P. Albertelli); 0000-0002-1957-3613 (M. Monno)



second one, where quantities of potential interest are measured from the machine tool, such as cutting forces, spindle torque, etc. (Kurada and Bradley (1997)). Despite the first methods provide accurate assessments of the tool condition (based on vision systems or proximity measurements, Zhu and Yu (2017)), they are limited in application since it is necessary to quit the machining operations and in most of the cases the measurements are time consuming (Kurada and Bradley (1997); Letot, Serra, Dossevi and Dehombreux (2015)). Thus, in the recent years, the main contributions have regarded indirect TCM methods, due to their in-process applicability. Most of the indirect TCM applications exploit cutting forces (and related quantities, Zhang, Gao, Guo, Zhang, Yin and Zhao (2023)), vibration measurements (Cheng, Jiao, Shi, Wang, Yan and Li (2020)) or acoustic emission signals (Zhou et al. (2021); Wang, Song, Liu, Ma and Liu (2022); Wickramarachchi, Rogers, McLeay, Leahy and Cross (2022)) in order to track the condition of the tool (Kuntoğlu et al. (2020a)). Many different machining applications have been investigated: drilling (Jiménez, Arizmendi and Sánchez (2021)), turning (Cheng et al. (2020); Letot et al. (2015)) and milling (Meng, Zhang, Xiao, Chen, Yi and Xu (2021); Jozić, Lela and Bajić (2014); Zhang et al. (2021); Stavropoulos et al. (2016)). Cutting forces are typically measured through dynamometric plates, which are not affordable for an industrial implementation (Baur et al. (2020)). To avoid the use of dynamometers, indirect methods for cutting forces estimation (Albertelli et al. (2016)) and novel integrated sensors (Zhang, Gao, Lu, Wang and Liao (2022a)) were developed and proposed. In order to extract wear related information, several feature extraction strategies can be applied to the measurements from time (e.g. mean, skewness and root mean square, Li and Zhu (2021)), frequency (e.g. maximum amplitude and average amplitude) or time-frequency domains (e.g. energy of each decomposed wavelet) (Meng et al. (2021); Zhang et al. (2021)). Such features are then fed into anomaly detection algorithms (monitoring), classification algorithms (diagnostics) or regression models (prognostics) (Bernini, Waltz, Albertelli and Monno (2021)). Nevertheless, the above traditional tool wear features are strongly influenced by the machining parameters. Thus, they can be applied only under fixed milling parameters (Pan, Zhang, Zhang, Zhao, Zhang and Lu (2022)). In recent studies, most of the approaches makes use of machine learning (Stavropoulos et al. (2016)) or deep learning algorithms, such as Convolutional Neural Networks (Zhang et al. (2021)). Since a large set of high-quality data taken in a wide range of cutting conditions is requested, their application to real industrial scenarios is challenging (Guo, Zhang, Peng, Zhuang, Wu and Zhang (2022); Li, Liu, Yue, Liang and Wang (2022)).

Consequently, the necessity to develop solutions based on process modelling, either physical or mechanistic is evident. From this perspective, different models with various grades of complexity have been used in literature to predict the cutting forces for a given machining operation. Physical-based approaches are based on slip-line field analysis to model the chip formation mechanism (e.g. (Fang, Jawahir and Oxley (2001))); an extended review of state-of-art approaches of this kind can be found in (Arrazola, Özel, Umbrello, Davies and Jawahir (2013)). Conversely, mechanistic models exploit simplified description of the process, but model coefficients (specific force coefficients, SFC) need to be experimentally identified (Altintas (2012)). The main feature of the SFC is that they are theoretically independent from some process parameters. At the same time, by representing the material shearing, the friction and ploughing effects involved in the cutting process, they carry the information about tool wear, becoming a relevant resource for TCM. Anyway, their identification is still based on multivariate linear regression on mean cutting forces measured during variable feed milling tests (Altintas (2012)). The Altintas model was widely studied and even upgraded with some additional features, such as improved chip thickness formulation including cutter run-out and cycloidal path (Kumanchik and Schmitz (2007); Matsumura and Tamura (2017)) or the inclusion of tool wear modelling in cutting forces expressions (Zhu and Zhang (2019); Liu, Liu, Zhao, Song, Ren and Ma (2022)), while several researches analyzed SFC dependence with respect to the cutting parameters in multiple applications: square shoulder mills (Nouri, Fussell, Ziniti and Linder (2015); Campatelli and Scippa (2012)) and ball-end milling (Guo, Wei, Wang, Li and Liu (2018)). Nouri *et al.* estimated such coefficients (exploiting mean forces) online during run-to-failure experiments. This was possible since cutting was executed continuously varying the feed per tooth, that cannot be guaranteed in real production scenarios (Nouri et al. (2015)). To overcome this limitation, new approaches based on the identification of SFC from instantaneous cutting forces were developed and tested (Farhadmanesh and Ahmadi (2021)). Nevertheless, up to the authors' knowledge, no-one still demonstrated the efficacy of such approaches for the real-time identification of SFC from instantaneous cutting forces in run-to-failure experiments and considering multiple cutting conditions.

Our research is intended to verify the applicability of SFC identification from instantaneous cutting forces in a TCM context. The paper structure is organized as follows. In section 2, the whole methodology is presented. A background of the mechanistic model for square shoulder mills and an innovative mechanistic formulation for high-feed mills are reported in sections 2.1 and 2.2. The SFC identification through multivariate linear regression and principal component regression are discussed in sections 2.3 and 2.4, respectively. Self-starting tabular cusum control charts for the detection

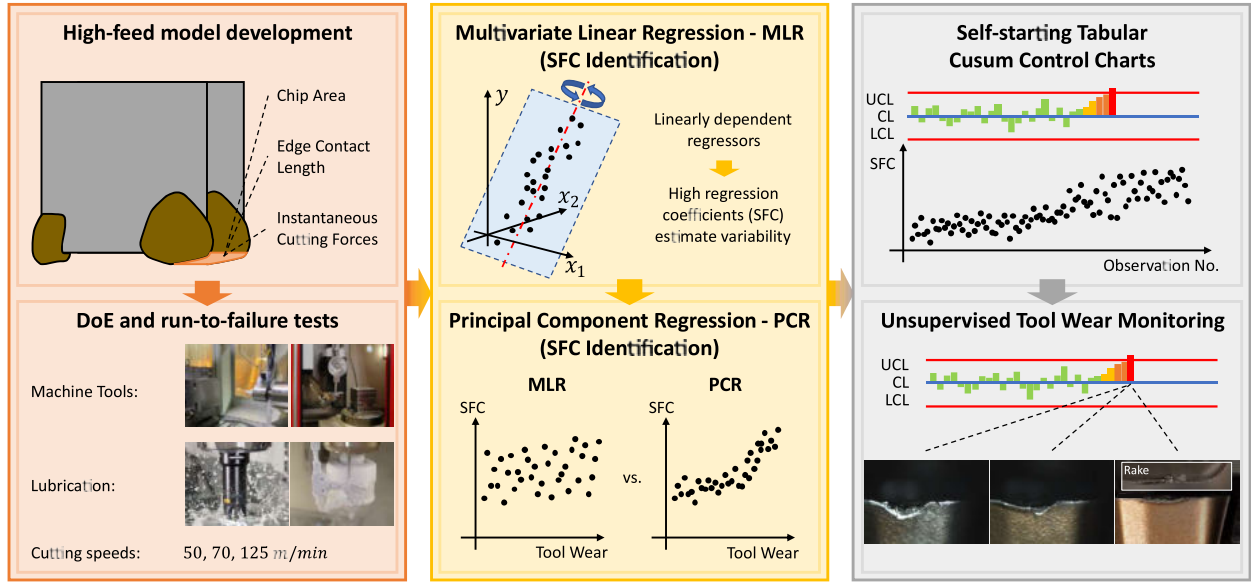


**Figure 1:** Overall framework of the work. Left branch represents the high-feed cutters used and the experimental campaign parameters. Middle branch shows the comparison between the methods used for Specific Force Coefficients identification. Right branch shows the application of control charts for the unsupervised tool wear monitoring of critical tool chipping and notch wear.

of out of control cutting processes are reported in section 2.5. In section 3 the experimental set-up and campaign are described. In section 4, the application of the conceived approach to the experimental data is presented and discussed with respect to the specific literature. In section 5, the main introduced novelties are highlighted and future works are outlined.

## 2. Methods

For sake of clarity, the approach adopted in this work is summarized in figure 1. The paper materials are summarized in the left branch of the figure, including a representation of the cutting tool and the experimental campaign (with two machine tools, conventional and cryogenic lubrication, and variable cutting speeds). The identification methods for the SFC are presented in the middle branch, while the goal of the proposed work is shown in the right branch of figure 1. In the following sections, all these points are thoroughly explained.

### 2.1. Theoretical background

The proposed solution is based on the identification of SFC during high-feed mill tests. Since a reliable mechanistic model for such mills is still not available, a specific formulation starting from (Altintas (2012)) is developed and here presented. The mill cutter positions are described in time through equation (1):

$$\varphi_i(t) = \varphi_0 + \frac{2\pi i}{N} + 2\pi n t, \quad i = 1, \dots, N \quad (1)$$

where  $\varphi_i$  is the angular position of the  $i$ -th cutter in the x-y reference plane (fig. 2);  $i$  is the cutter identifier;  $t$  is time;  $\varphi_0$  is the initial phase of the first cutter;  $N$  is the number of teeth of the mill and  $n$  is its rotational speed. From now on, the time dependence is neglected. Altintas defines the instantaneous thickness  $h$  of the chip removed by a cutter as a function of the feed per tooth  $c$ , eq. (2):

$$h(\varphi) = c \sin \varphi \quad (2)$$

The expression for the tangential and radial cutting forces on a cutter, keeping in consideration the engagement conditions, are given by equation (3):

$$F_t = g(\varphi) (K_{tc} a h + K_{te} a)$$

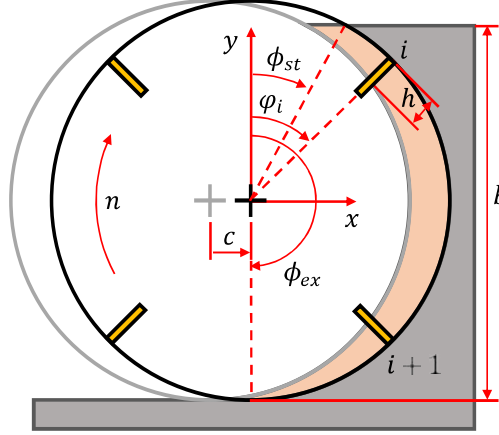


Figure 2: Reference model for the geometry of milling operations.

 Table 1  
Cutter geometrical parameters.

$r_{1c}$ [mm]	$r_{2c}$ [mm]	$r_{3c}$ [mm]	$z_1$ [mm]	$z_2$ [mm]	$z_3$ [mm]
6.57	8.53	9.03	0	0.40	0.62

$$F_r = g(\varphi) (K_{rc} a h + K_{re} a) \quad (3)$$

where  $F_t$  and  $F_r$  are the tangential and radial forces acting on a single cutter;  $K_{tc}$ ,  $K_{te}$ ,  $K_{rc}$  and  $K_{re}$  are the SFC: the first and second are the tangential ones, the third and fourth are the edge ones;  $a$  is the axial depth of cut;  $g(\varphi)$  is the engagement function defined by eq. (4):

$$g(\varphi) = \begin{cases} 1, & \text{if } \phi_{st} < \varphi < \phi_{ex} \\ 0, & \text{otherwise.} \end{cases} \quad (4)$$

and  $\phi_{st}$ ,  $\phi_{ex}$  are the entry and exit angles determined by the engagement conditions of the mill (e.g. for downmilling, they are expressed by eq. (5)):

$$\begin{aligned} \phi_{st} &= \pi - \arccos\left(1 - \frac{2b}{D}\right) \\ \phi_{ex} &= \pi \end{aligned} \quad (5)$$

where  $b$  is the radial depth of cut;  $D$  is the diameter of the mill.

The single cutter contributions must then be projected on the x-y reference frame and summed up (eq. (6)):

$$\begin{aligned} F_x &= \sum_{i=1}^N (-F_{t,i} \cos \varphi_i - F_{r,i} \sin \varphi_i) \\ F_y &= \sum_{i=1}^N (+F_{t,i} \sin \varphi_i - F_{r,i} \cos \varphi_i) \end{aligned} \quad (6)$$

## 2.2. High-feed model

In this paper the experimental campaign was conducted using high-feed mills, featured by a double-phased profile. Their shape is schematically shown in figure 3a. The proposed high-feed mechanistic model makes reference to figure 3a, from which the maximum allowable chip shape is derived. This shape corresponds to the region comprised between the current and previous tooth profiles, shifted by the chip thickness  $h$ . In order to describe the chip shape, it is necessary

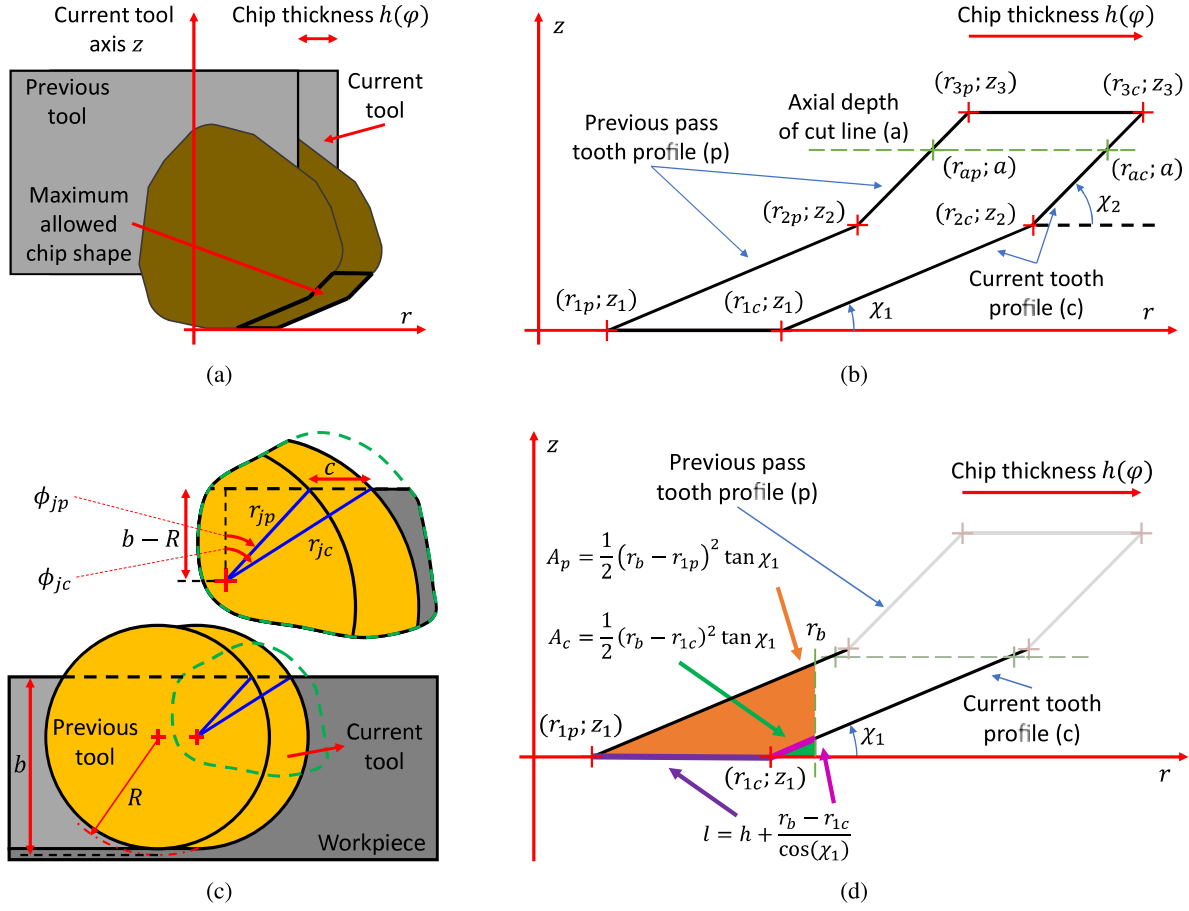


**Figure 3:** Reference figure for the high-feed model: (a) derivation of the maximum allowable chip shape; (b) maximum allowable chip shape and high-feed cutter reference points; (c) derivation scheme for current and previous critical angles; (d) derivation scheme for current and previous chip area and chip edge length for an example case ( $a \leq z_2$ ,  $\phi_{1p} \leq \varphi \leq \phi_{ap}$ ).

to define the cutter geometry. The geometry of the profile is uniquely defined in the radial-axial plane ( $r$ - $z$ ), figure 3b. The quantities  $r_{1c}$ ,  $r_{2c}$ ,  $r_{3c}$ ,  $z_1$ ,  $z_2$  and  $z_3$  are known for a given high-feed cutter, and they represent the radial and axial coordinates of the current (c) cutter fundamental points, defining the two phases of the cutting edge;  $\chi_1$  and  $\chi_2$  are the lead angles of the two cutter phases. The values associated to the cutters used for the experimentation are reported in table 1. The intersection of the axial depth of cut ( $a$ ) line with the cutter geometry originates another important point, having coordinates  $(r_{ac}; a)$ , given by eq. (7):

$$r_{ac} = \begin{cases} r_{1c} + \frac{a}{\tan \chi_1}, & \text{if } a \leq z_2 \\ r_{2c} + \frac{a - z_2}{\tan \chi_2}, & \text{if } z_2 < a \leq z_3 \end{cases} \quad (7)$$

$r_{1p}$ ,  $r_{2p}$ ,  $r_{3p}$  and  $r_{ap}$  are the radial coordinates of the analogous points on the previous (p) cutter profile (i.e. related to the previous pass), and thus, they are determined through eq. (8):

$$r_{jp}(\varphi) = r_{jc} - h(\varphi), \quad j = 1, 2, 3, a \quad (8)$$

where  $r_{jp}$  is a function of the position of the correspondent cutter angle  $\varphi$ ; for the sake of conciseness this dependence will be omitted in the following. The radial engagement of the cutter is given by the radial depth of cut  $b$ , here expressed with reference to the cutter nominal radius  $R$  (figure 3c). Thus, each of the current and previous fundamental points is

engaged when the cutter position reaches the critical corresponding angles  $\phi_{jc}$  and  $\phi_{jp}$  (eq. 9):

$$\begin{aligned}\phi_{jc} &= \arccos \frac{b-R}{r_{jc}} \\ \phi_{jp} &= \arctan \frac{r_{jc} \sin \phi_{jc} - c}{b-R}\end{aligned}\quad (9)$$

with  $j = 1, 2, 3, a$ . As a consequence, when a cutter position overcomes one of these angles, the chip shape changes. [These relations are easily determined from the scheme reported in figure 3c through trigonometry.](#)

It is important to define the actual radial engagement of a tooth  $r_b(\varphi)$ , given its current position (eq. 10):

$$r_b(\varphi) = \min \left( \frac{b-R}{\cos \varphi}, r_{ac} \right) \quad (10)$$

$r_b(\varphi)$  is initially limited by the workpiece (radial engagement) until it reaches the maximum engaged radial distance (determined by the axial depth of cut. The switch happens in correspondence of  $\varphi = \phi_{ac}$ . From here on, we will omit the  $\varphi$  dependences. All the above-mentioned variables are needed to compute the actual chip area  $A$  and edge contact length  $l$ , taking in consideration even the progressive radial engagement of the cutter.  $A$  and  $l$  are the results of the integration of the infinitesimal chip area  $dA$  and chip edge length  $dl$  (eq. (11)) over the radial coordinate from  $r_{1p}$  to  $r_b$ .

$$\begin{aligned}dA(r) &= [z_p(r) - z_c(r)] dr = dA_p(r) - dA_c(r) \\ dl(r) &= \frac{dr}{\cos \chi(r)}\end{aligned}\quad (11)$$

where  $z_p(r)$  is the axial coordinate of the point on the previous cutter profile at a generic radial distance  $r$  from the mill axis (fig. 3d);  $z_c(r)$  is the same as  $z_p(r)$ , but computed on the current cutter profile;  $dr$  is an infinitesimal variation in the radial direction;  $dA_p(r)$  and  $dA_c(r)$  are the infinitesimal areas below the previous and current tooth profile at radial coordinate  $r$ , respectively;  $\chi(r)$  is the lead angle at the  $r$  radial coordinate. Thus, eq. (3) is modified in equation (12) and then, it can be introduced in eq. (6):

$$\begin{aligned}F_t &= K_{tc} (A_p - A_c) + K_{te} l \\ F_r &= K_{rc} (A_p - A_c) + K_{re} l\end{aligned}\quad (12)$$

where  $F_t$ ,  $F_r$ ,  $A_p$ ,  $A_c$  and  $l$  dependencies on  $\varphi$  were omitted;  $A_p$ ,  $A_c$  and  $l$  are the integrals of the above-mentioned differentials  $dA_p$ ,  $dA_c$  and  $dl$ , respectively.  $A_p$ ,  $A_c$  and  $l$  must be defined for the two cases  $a \leq z_2$  and  $z_2 < a \leq z_3$ .

**Case I:  $a \leq z_2$**

The value of  $A_p$  is given by eq. (13):

$$A_p = \begin{cases} \frac{1}{2} (r_b - r_{1p})^2 \tan \chi_1, & \text{if } \phi_{1p} < \varphi \leq \phi_{ap} \\ \frac{1}{2} (r_{ap} - r_{1p}) a + (r_b - r_{ap}) a, & \text{if } \phi_{ap} < \varphi \leq \phi_{ac} \\ \frac{1}{2} (r_{ap} - r_{1p}) a + (r_{ac} - r_{ap}) a, & \text{if } \phi_{ac} < \varphi \leq \pi \\ 0, & \text{otherwise.} \end{cases} \quad (13)$$

While  $A_c$  is given by eq. (14):

$$A_c = \begin{cases} \frac{1}{2} (r_b - r_{1c})^2 \tan \chi_1, & \text{if } \phi_{1c} < \varphi \leq \phi_{ac} \\ \frac{1}{2} (r_{ac} - r_{1c}) a, & \text{if } \phi_{ac} < \varphi \leq \pi \\ 0, & \text{otherwise.} \end{cases} \quad (14)$$

$l$  is given by eq. (15):

$$l = \begin{cases} r_b - r_{1p}, & \text{if } \phi_{1p} < \varphi \leq \phi_{1c} \\ h + \frac{r_b - r_{1c}}{\cos(\chi_1)}, & \text{if } \phi_{1c} < \varphi \leq \phi_{ac} \\ h + \frac{r_{ac} - r_{1c}}{\cos(\chi_1)}, & \text{if } \phi_{ac} < \varphi \leq \pi \\ 0, & \text{otherwise.} \end{cases} \quad (15)$$

The example scheme for retrieving the first case of each of these terms is shown in figure 3d. Other cases can be obtained by moving  $r_b$  progressively towards higher values.

**Case 2:**  $z_2 < a \leq z_3$

The value of  $A_p$  is given by eq. (16):

$$A_p = \begin{cases} \frac{1}{2} (r_b - r_{1p})^2 \tan \chi_1, & \text{if } \phi_{1p} < \varphi \leq \phi_{2p} \\ \frac{1}{2} (r_{2c} - r_{1c}) z_2 + (r_b - r_{2p}) z_2 + \frac{1}{2} (r_b - r_{2p})^2 \tan \chi_2, & \text{if } \phi_{2p} < \varphi \leq \phi_{ap} \\ \frac{1}{2} (r_{2c} - r_{1c}) z_2 + \frac{1}{2} (r_{ap} - r_{2p}) (z_2 + a) + (r_b - r_{ap}) a, & \text{if } \phi_{ap} < \varphi \leq \phi_{ac} \\ \frac{1}{2} (r_{2c} - r_{1c}) z_2 + \frac{1}{2} (r_{ap} - r_{2p}) (z_2 + a) + (r_{ac} - r_{ap}) a, & \text{if } \phi_{ac} < \varphi \leq \pi \\ 0, & \text{otherwise.} \end{cases} \quad (16)$$

While  $A_c$  is given by eq. (17):

$$A_c = \begin{cases} \frac{1}{2} (r_b - r_{1c})^2 \tan \chi_1, & \text{if } \phi_{1c} < \varphi \leq \phi_{2c} \\ \frac{1}{2} (r_{2c} - r_{1c}) z_2 + (r_b - r_{2c}) z_2 + \frac{1}{2} (r_b - r_{2c})^2 \tan \chi_2, & \text{if } \phi_{2c} < \varphi \leq \phi_{ac} \\ \frac{1}{2} (r_{2c} - r_{1c}) z_2 + \frac{1}{2} (r_{ac} - r_{2c}) (z_2 + a), & \text{if } \phi_{ac} < \varphi \leq \pi \\ 0, & \text{otherwise.} \end{cases} \quad (17)$$

$l$  is given by eq. (18):

$$l = \begin{cases} r_b - r_{1p}, & \text{if } \phi_{1p} < \varphi \leq \phi_{1c} \\ h + \frac{r_b - r_{1c}}{\cos(\chi_1)}, & \text{if } \phi_{1c} < \varphi \leq \phi_{2c} \\ h + \frac{r_{2c} - r_{1c}}{\cos(\chi_1)} + \frac{r_b - r_{2c}}{\cos(\chi_2)}, & \text{if } \phi_{2c} < \varphi \leq \phi_{ac} \\ h + \frac{r_{2c} - r_{1c}}{\cos(\chi_1)} + \frac{r_{ac} - r_{2c}}{\cos(\chi_2)}, & \text{if } \phi_{ac} < \varphi \leq \pi \\ 0, & \text{otherwise.} \end{cases} \quad (18)$$

It must be noted that the proposed model uses a circular approximation of the tooth trajectory. This choice was based on the fact that high-feed mills may reach up to ten times conventional milling *feed over mill radius ratios* (Duplak, Hatala, Duplakova and Steranka (2018)), but they present a relatively low *non dimensional cutting parameter* (Kumanchik and Schmitz (2007)), not comparable with micro milling ones. In case of really aggressive cutting processes, actual tool tip trajectory can be introduced following Kumanchik and Schmitz (2007) and Farhadmanesh and Ahmadi (2021). Nevertheless, critical angles in equation (9) must be adapted accordingly.

### 2.3. SFC identification

The identification of SFC is typically carried out by a multivariate linear regression based on average cutting forces in milling tests with variable feed per tooth. This procedure is well established in literature and references for performing such identification can be found in Altintas (2012) as well as in Farhadmanesh and Ahmadi (2021).

In this paper, the fitting procedure was based on instantaneous cutting forces, following a procedure proposed by Farhadmanesh and Ahmadi (2021). SFC estimation is performed every 3 tool revolutions (where, 3 was chosen to keep the SFC estimation reliable), and the estimation number is indicated with the  $o$  index. For each estimation,  $N_s$  measurement samples are used and index  $s$  will indicate the sample number for the  $o$ -th estimate. Thus, for a given

estimate number  $o$ ,  $s$  will range from 1 to  $N_s$ .  $o$  ranges from estimation number 1 to the total number of estimates  $N_o$ . The model for the  $o$ -th SFC estimate is represented by eq. (19):

$$\mathbf{y}^{(o)} = \mathbf{X}^{(o)} \boldsymbol{\beta}^{(o)} + \boldsymbol{\epsilon}^{(o)} \quad (19)$$

where  $\mathbf{y}^{(o)}$  is the response vector;  $\mathbf{X}^{(o)}$  is the design matrix;  $\boldsymbol{\beta}^{(o)}$  is the vector of regression coefficients and  $\boldsymbol{\epsilon}^{(o)}$  is the vector of residuals (Montgomery (2012)) that considers the modelling errors. The elements of  $\boldsymbol{\epsilon}^{(o)}$  are assumed to be drawn from an uncorrelated random variable and  $\boldsymbol{\epsilon}^{(o)}$  is assumed to have null expected value and variance  $\sigma^2$ . The response vector  $\mathbf{y}^{(o)}$  is a  $2N_s \times 1$  vector containing instantaneous cutting forces as in eq. (20):

$$\mathbf{y}^{(o)} = \{F_{x,1} \ F_{x,2} \ \dots \ F_{x,N_s} \ F_{y,1} \ F_{y,2} \ \dots \ F_{y,N_s}\}^T \quad (20)$$

The column vector  $\boldsymbol{\beta}^{(o)}$  of regression coefficients contains the SFC to be identified at the  $o$ -th estimation instant (eq. (21)):

$$\boldsymbol{\beta}^{(o)} = \left\{ K_{tc}^{(o)} \ K_{te}^{(o)} \ K_{rc}^{(o)} \ K_{re}^{(o)} \right\}^T \quad (21)$$

The design matrix at  $o$  estimation number is derived by stacking column-wise the matrix in eq. (22) for each of the  $N_s$  instants, resulting in a  $2N_s \times 4$  design matrix:

$$\mathbf{x}_s = \begin{bmatrix} x_{11s} & x_{12s} & x_{13s} & x_{14s} \\ x_{21s} & x_{22s} & x_{23s} & x_{24s} \end{bmatrix} \quad (22)$$

where the single elements are reported in eq. (23):

$$\begin{aligned} x_{11s} &= - \sum_{i=1}^N A(\varphi_{is}) \cos \varphi_{is} \\ x_{12s} &= - \sum_{i=1}^N l(\varphi_{is}) \cos \varphi_{is} \\ x_{13s} &= - \sum_{i=1}^N A(\varphi_{is}) \sin \varphi_{is} \\ x_{14s} &= - \sum_{i=1}^N l(\varphi_{is}) \sin \varphi_{is} \\ x_{21s} &= \sum_{i=1}^N A(\varphi_{is}) \sin \varphi_{is} \\ x_{22s} &= \sum_{i=1}^N l(\varphi_{is}) \sin \varphi_{is} \\ x_{23s} &= - \sum_{i=1}^N A(\varphi_{is}) \cos \varphi_{is} \\ x_{24s} &= - \sum_{i=1}^N l(\varphi_{is}) \cos \varphi_{is} \end{aligned} \quad (23)$$

where  $A = A_p - A_c$  and  $l$  are the high-feed chip area and edge contact length. The least square solution for this problem gives the  $o$ -th estimation of the SFC, eq. (24):

$$\hat{\boldsymbol{\beta}}^{(o)} = (\mathbf{X}^{(o)T} \mathbf{X}^{(o)})^{-1} \mathbf{X}^{(o)T} \mathbf{y}^{(o)} \quad (24)$$



thus, the SFC ( $\hat{\beta}^{(o)}$ ) estimated through this formula will be indicated as  $\hat{K}_{tc}^{(o)}$ ,  $\hat{K}_{te}^{(o)}$ ,  $\hat{K}_{rc}^{(o)}$  and  $\hat{K}_{re}^{(o)}$ . Actually, at the beginning of each cut, the initial tool phase  $\varphi_0$  is unknown. The estimation of  $\varphi_0$  can be obtained solving  $N_q$  regressions with a different tool phase  $\varphi_{0q}$  (eq. (25)):

$$\varphi_{0q} = \frac{2\pi}{N} \frac{q}{R}, \quad q = 1, \dots, N_q \quad (25)$$

The regression with minimum least square error gives the best estimates for  $\varphi_0$  and SFC (Farhadmanesh and Ahmadi (2021)).

#### 2.4. Principal Components Regression

As it will be explained in section 4, the  $\hat{\beta}$  estimation (for this particular problem) tends to suffer from the multicollinearity phenomenon, which turns into a high variability of the estimated regression coefficients. In order to limit this effect, Principal Components Regression (PCR) was introduced (Hintze (2007)). PCR performs a multivariate linear regression on a subset of principal components of the design matrix. At first, each column of the design matrix and the response vector are standardized to have null mean and unitary standard deviation (Hastie, Tibshirani and Friedman (2009)), bringing to the  $\tilde{\mathbf{X}}$  matrix and  $\tilde{\mathbf{y}}$  vector (omitting  $o$  dependency, eq. (26)):

$$\tilde{\mathbf{X}} = \begin{bmatrix} \frac{x_1 - \bar{x}_1}{\sigma_{x_1}} & \frac{x_2 - \bar{x}_2}{\sigma_{x_2}} & \frac{x_3 - \bar{x}_3}{\sigma_{x_3}} & \frac{x_4 - \bar{x}_4}{\sigma_{x_4}} \end{bmatrix} \quad \tilde{\mathbf{y}} = \frac{y - \bar{y}}{\sigma_y} \quad (26)$$

Then, PCA is performed on the matrix  $\tilde{\mathbf{X}}$ . This is achieved through the computation of the eigenvalues  $\lambda$  and eigenvector matrix  $\mathbf{V}$  of the covariance matrix  $\Sigma$  of  $\tilde{\mathbf{X}}$ . The standardized design matrix  $\tilde{\mathbf{X}}$  is projected on the principal components (PCs) directions by eq. (27):

$$\mathbf{Z} = \mathbf{X}\mathbf{V} \quad (27)$$

The principal components matrix  $\mathbf{Z}$  is then used to perform a multivariate linear regression on the response vector  $\tilde{\mathbf{y}}$ . The  $o$ -th regression coefficients estimate performed by PCR (eq. (28)) is  $\tilde{\alpha}_{full}^{(o)}$ :

$$\tilde{\alpha}_{full}^{(o)} = (\mathbf{Z}^{(o)T} \mathbf{Z}^{(o)})^{-1} \mathbf{Z}^{(o)T} \tilde{\mathbf{y}}^{(o)} \quad (28)$$

At this point, it is necessary to remove the PCs with the lowest eigenvalues (i.e. the ones describing the lowest part of variability in the data). This is achieved by setting the last elements of  $\tilde{\alpha}_{full}^{(o)}$  to zero and obtaining  $\tilde{\alpha}_{PCR}^{(o)}$  (Hintze (2007)). In the studied case, two coefficients are set to zero, eq. (29):

$$\tilde{\alpha}_{PCR}^{(o)} = \left\{ \tilde{\alpha}_{1,full}^{(o)} \quad \tilde{\alpha}_{2,full}^{(o)} \quad 0 \quad 0 \right\}^T \quad (29)$$

Finally, it is possible to transform  $\tilde{\alpha}_{PCR}^{(o)}$  back to the original space through eq. (30):

$$\tilde{\beta}_{std}^{(o)} = \mathbf{V}^{(o)} \tilde{\alpha}_{PCR}^{(o)} \quad (30)$$

Due to the standardization of the data, the estimated coefficients must be scaled to match the original dimensions. The transformation gives the final set of regression coefficients  $\tilde{\beta}^{(o)}$  and it is given by eq. (31):

$$\tilde{\beta}^{(o)} = \left\{ \frac{\tilde{\beta}_{1,std}^{(o)}}{\sigma_{x_1}^{(o)}} \quad \frac{\tilde{\beta}_{2,std}^{(o)}}{\sigma_{x_2}^{(o)}} \quad \frac{\tilde{\beta}_{3,std}^{(o)}}{\sigma_{x_3}^{(o)}} \quad \frac{\tilde{\beta}_{4,std}^{(o)}}{\sigma_{x_4}^{(o)}} \right\}^T \sigma_y^{(o)} \quad (31)$$

thus, the SFC ( $\tilde{\beta}^{(o)}$ ) estimated through this method will be called as  $\tilde{K}_{tc}^{(o)}$ ,  $\tilde{K}_{te}^{(o)}$ ,  $\tilde{K}_{rc}^{(o)}$  and  $\tilde{K}_{re}^{(o)}$ .



## 2.5. Self-starting Tabular Cusum control chart

The regression coefficients become here the object of the monitoring strategy. As it will be explained in section 4, the  $\tilde{K}_{re}$  coefficient is the most stable and correlated to the tool wear. Here, it will be used as a tool wear indicator to be monitored. Following the work by Farhadmanesh *et al.* the moving range related to the  $\tilde{K}_{re}^{(o)}$  estimation is computed through eq. (32) (Farhadmanesh and Ahmadi (2021)):

$$MR_o = |\tilde{K}_{re,o} - \tilde{K}_{re,o-1}| \quad (32)$$

The moving range is then averaged on 15 samples batches (eq.(33)), leading to the variable  $v_n$ :

$$v_n = \sum_{o=1}^{15} \frac{MR_o}{15} \quad (33)$$

$v_n$  is then fed to a self-starting tabular Cusum control chart (Montgomery (2008)). First of all, the running average is updated as soon as the  $n$ -th observation  $v_n$  becomes available (eq.(34)):

$$\bar{v}_n = \bar{v}_{n-1} + \frac{v_n - \bar{v}_{n-1}}{n} \quad (34)$$

The sum of squared deviations is updated, too (eq.(35)):

$$w_n = w_{n-1} + \frac{(n-1)(v_n - \bar{v}_{n-1})^2}{n} \quad (35)$$

The running standard deviation becomes (eq.(36)):

$$s_n = \sqrt{\frac{w_n}{n-1}} \quad (36)$$

The  $n$ -th observation is then standardized through eq. (37):

$$T_n = \frac{v_n - \bar{v}_{n-1}}{s_{n-1}} \quad (37)$$

It turns out that the quantity  $U_n$  is distributed as a standard normal random variable (if the monitored variable  $v$  is normally distributed), where  $U_n$  is defined by eq. (38):

$$U_n = \Phi^{-1} [CDF_{t,n-2} (a_n T_n)] \quad (38)$$

where  $\Phi^{-1}(\cdot)$  is the inverse normal cumulative distribution;  $CDF_{t,n-2}(\cdot)$  is the cumulative  $t$  distribution with  $n-2$  degrees of freedom;  $a_n = \sqrt{\frac{n-1}{n}}$  (Montgomery (2008)). Thus, it is possible to apply the tabular Cusum control chart on  $U_n$ .

The Cusum control chart is based on the computation of two cumulative derivation with above and below the target value,  $C_n^+$  and  $C_n^-$ , respectively. They are initialized to be null:  $C_0^+ = 0$  and  $C_0^- = 0$ . Every time a  $U_n$  becomes available, the following expressions are computed (eq.(39)):

$$\begin{aligned} C_n^+ &= \max [0, U_n - (\mu_0 + K) + C_{n-1}^+] \\ C_n^- &= \max [0, (\mu_0 - K) - U_n + C_{n-1}^-] \end{aligned} \quad (39)$$

where  $K$  is typically set to  $\frac{1}{2}\sigma_0$ ;  $\mu_0$  and  $\sigma_0$  are the mean and standard deviation of  $U$  random variable, thus  $\mu_0 = 0$  and  $\sigma_0 = 1$ . The process is considered out of control when either  $C_n^+$  or  $C_n^-$  overcome the threshold  $H$ , commonly set to  $5\sigma_0$  (Montgomery (2008)).

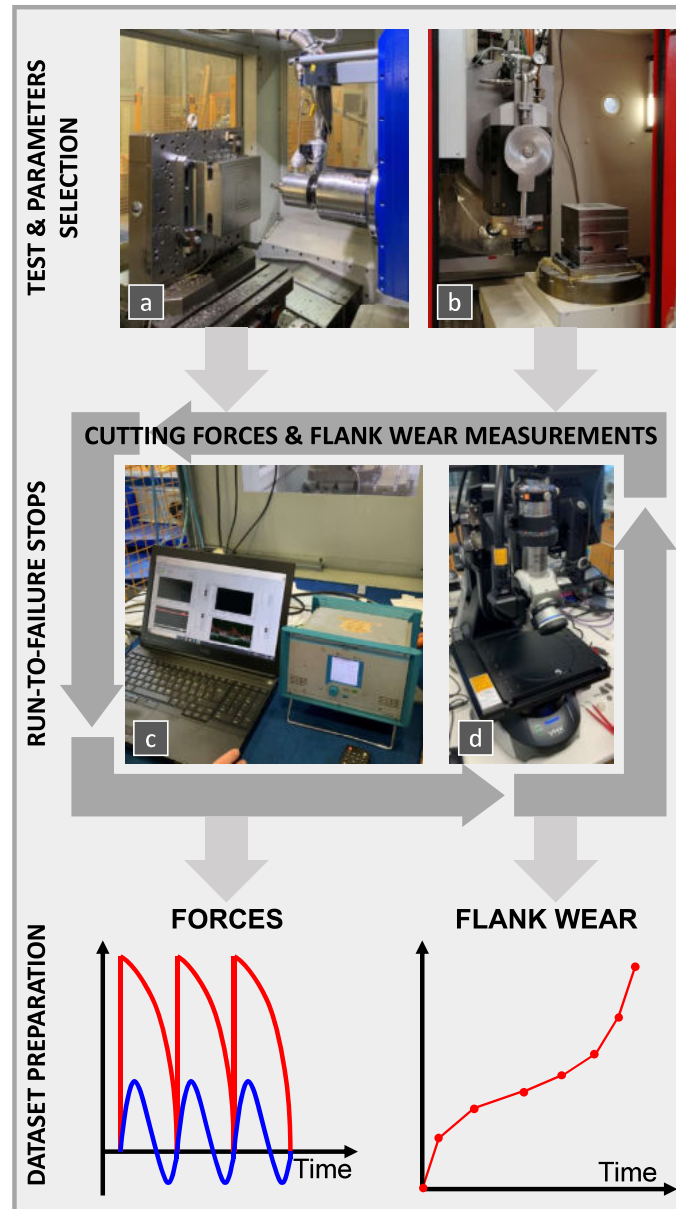


**Figure 4:** Experimental set-up: a) Mandelli M5, Mitsubishi mill, Kistler dynamometer and cryogenic set-up; b) Sigma Flexi FFG group, Mitsubishi mill, Kistler dynamometer and conventional cooling set-up; c) DAQ system; d) Keyence microscope. Run-to-failures are performed through stops, in order to assess the flank wear.

### 3. Materials

The experimental session was carried out on two different machine tools: a Mandelli M5 machine tool and a Sigma Flexi FFG group machine tool; both of them, featuring a Mitsubishi AJX06R203SA20S high-feed mill, with three JOMT06T216ZZER-JL MP9140 cutting inserts. The available set-ups were presented in figure 4. During the milling test, Kistler 9255B dynamometric plate was adopted to measure the cutting forces during the milling operations. The dynamometer was connected to Kistler 5070A charge amplifier (fig. 4c). The cutting forces were acquired through a NI cDAQ- 9174, with a NI 9215 acquisition card. The sampling frequency of the acquisition was set to  $5kHz$ . For the inspection of wear on cutters, a Keyence VHX-7000 microscope was used (fig. 4d).

**Table 2**  
Design of Experiments

Test	$v_c$ [m/min]	$n$ [rpm]	$v_f$ [mm/min]	Lubrication	Machine
1	50	796	1671	Cryogenic	Flexi
2	70	1114	2340	Cryogenic	Flexi
3	70	1114	2340	Lubricant	Flexi
4	125	1989	4178	Lubricant	M5
5	125	1989	4178	Cryogenic	M5

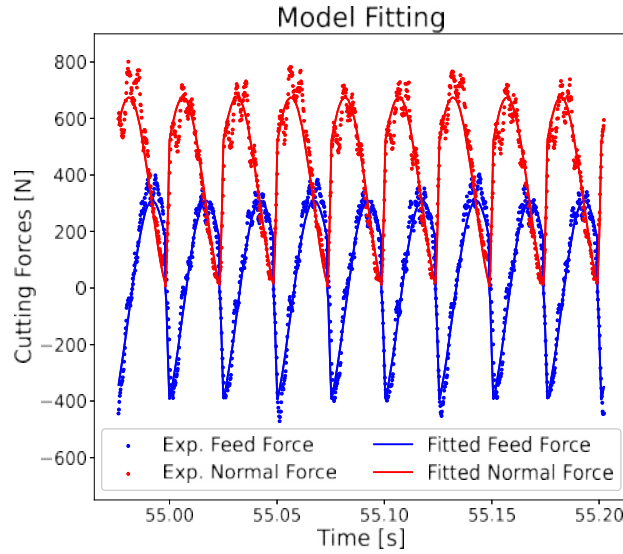


**Figure 5:** Comparison between the  $\alpha$ -th fitted instantaneous cutting forces and the  $\alpha$ -th experimentally measured ones (thus including 3 mill revolutions). The example set of forces was taken from test 1: Flexi machine tool,  $v_c = 50$  m/min,  $c = 0.7$  mm/tooth, cryogenic,  $n = 796$  rpm,  $v_f = 1671$  mm/min.

The experimentation consisted of 5 run-to-failure tests (i.e. machining the workpiece until the cutters were completely worn out). The run-to-failure experiments were performed until either mean flank wear reached  $300\mu\text{m}$  or maximum flank wear reached  $600\mu\text{m}$ . The acquisition of the experimental tests was subdivided in subsequent steps in order to perform the flank wear assessment (fig. 4). The workpiece consisted of a  $255 \times 262$  mm block made of  $Ti_6Al_4V$ , grade 5. The experimentation was carried out in different cutting conditions, i.e. changing machine tool (M5 and Flexi), cutting speed ( $50$  m/min,  $70$  m/min and  $125$  m/min) and lubrication set-ups (lubricant and cryogenic). The axial depth of cut  $a$  was set to  $0.4$  mm, the radial depth of cut  $b$  was set to  $13$  mm, while the feed per tooth  $c$  was fixed to  $0.7$  mm. The cutting test descriptive data are reported in table 2.

## 4. Results and discussion

### 4.1. SFC estimation and cutting forces prediction

The novel high-feed mill formulation was fitted on the whole dataset of experimental data. Since the fitting procedure worked on instantaneous cutting forces, the accuracy of the model in the time interval used to retrieve the SFC is really high. An example of fitted cutting forces, compared with experimentally measured forces is reported in figure 5. For the example set of forces (taken from test 1), the R-squared was equal to 0.979 (following R-squared definition for regression through the , Eisenhauer (2003)). Obviously, the high fitting capability of the instantaneous cutting forces-based procedure, is constrained to the time interval in which it is computed. The prediction capabilities

### Unsupervised TCM based on specific force coefficients

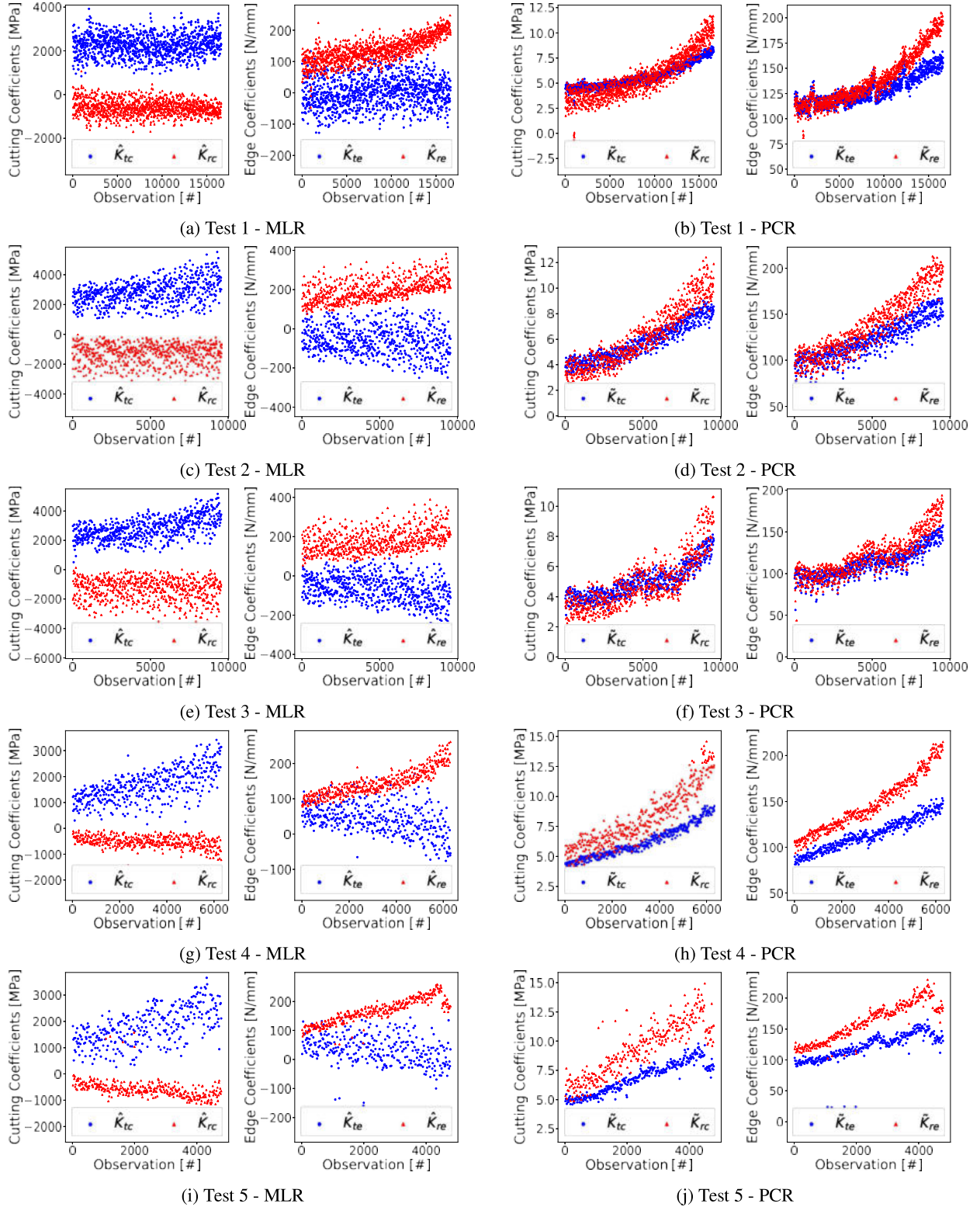


**Figure 6:** Evolution of the specific force coefficients during the execution of tests. SFC on the left are obtained through multivariate linear regression (MLR) and ordinary least squares solution. SFC on the right are obtained through Principal Component Regression (PCR).

may be comparable or slightly worse than an average cutting forces-based procedure in terms of forecasting new cutting forces, especially when different cutting parameters are used. Nonetheless, for the conceived unsupervised approach, we are interested on a local/instantaneous estimation of SFC (i.e. regression coefficients), not in the prediction of new cutting forces.

## 4.2. MLR and PCR comparison

In figure 6, we represented the evolution of the considered four SFC along the execution of all the tests using MLR and PCR. Figures 6a, 6c, 6e, 6g and 6i showed the evolution of the SFC estimated through ordinary least squares solution of multivariate linear regression. It can be noted that the identification of SFC through this method suffers of high variability. This effect is linked to a multicollinearity phenomenon. [Such phenomenon occurs when the regressors \(i.e. the columns of the design matrix\) tend to be linearly dependent one with respect to the other.](#) This translates in a large variance in the estimation of regression coefficients. The multicollinearity problem is typically solved by implementing biased regression methods. In general, these methods dramatically reduce the estimation variance of the regression coefficients, hopefully leading to a better bias-variance trade-off on the estimation; thus, to a more reliable estimation of the SFC. Here, as described in section 2, we proposed the Principal Component Regression algorithm, to reduce the variance associated to the estimated SFC. The output of PCR is presented for all the tests in figures 6b, 6d, 6f, 6h and 6j. It must be noted, how PCR enhanced the reliability of the SFC estimation (i.e. by reducing the estimation variability), providing an intrinsic highlight of the wear phenomenon. On the other hand, PCR introduced a high bias in the cutting SFC (i.e.,  $\tilde{K}_{tc}$  and  $\tilde{K}_{rc}$ ) which were reduced of almost three orders of magnitude. This is a result of the dimensionality reduction implemented by PCR; forgetting about the last two principal components (as explained in section 2), caused the cutting coefficient contributions to be almost removed. Furthermore, it is evident that  $\tilde{K}_{re}$  is the coefficient presenting early signs and higher correlation with respect to tool degradation. This was expected and in agreement with literature analysis developed on mean forces-based estimation approaches, such as in Nouri et al. (2015).

## 4.3. Tool wear detection

[Based on the results presented in section 4.2,](#) it was decided to apply the self-starting control charts directly on  $\tilde{K}_{re}$ , as explained in section 2. The application of this kind of control charts allowed to build a completely unsupervised strategy to monitor the tool wear status along run-to-failures. In fact, they don't need a design phase to determine the variability and target of the monitored variable, but they are developed such that they estimate them as long as the data become available. The results of the application of self-starting control charts on the  $\tilde{K}_{re}$  moving range on the full set of tests are shown in figure 7. [The figure for each experimental test the computed self-starting control chart main quantities. The red bar represents the first out of control observation of the process.](#) Control charts graphs are accompanied by the flank wear and, if relevant, rake crater pictures at the stop before (pictures in the middle) and after (pictures on the right) the detection, in order to highlight the meaning of an out of control observation. The evolution of the mean moving range (blue triangles) in figure 7 presents two different regions: a first stage, related to the initial tool life, where this coefficient is more or less stable, similar to the aspect of a random variable; a second stage with an increasing trend, higher variance and outliers. This behaviour is in agreement with the results found by Nouri et al., who observed that the mean moving range of the  $K_{re}$  (estimated through a mean forces-based approach) faced a dramatic change in variance after a given number of performed cuts. They reported that this change in the behaviour of the moving range was correlated to either the occurrence of chipping on the cutting edge of tool inserts or a 3-dimensional evolution of the wear zone on the tool insert (Nouri et al. (2015)). This was due to the sum of variations of infinitesimal cutting force directions along the worn cutting edges. The pictures of the cutting tool edges in figure 7 seem to be in agreement with the same hypothesis. The detection of the out of control observation falls in between the two stops corresponding to the proposed middle and right images. For what concerns tests 1, 2 and 3, the detection occurs when the cutting edge starts to feature an enhanced V wear shape, which is a 3D geometrical feature connecting the rake and flank faces (figures 7a, 7b and 7c). This phenomenon is associated to the occurrence of notch wear. After an initial period of regular flank land increase, localized accumulation of damages due to adhesion modify the cutting edge geometry leading to the formation of a notch. The notch is a 3D geometrical feature connecting the crater and the flank land and can be identified from a V shape on the flank surface. The proposed monitoring algorithm detects an out of control point when the notch wear starts to become critical. Regarding tests 4 and 5, the cutting inserts feature small chippings on the flank face, accompanied by bigger chippings on the rake face (as can be seen in figures 7d and 7e).



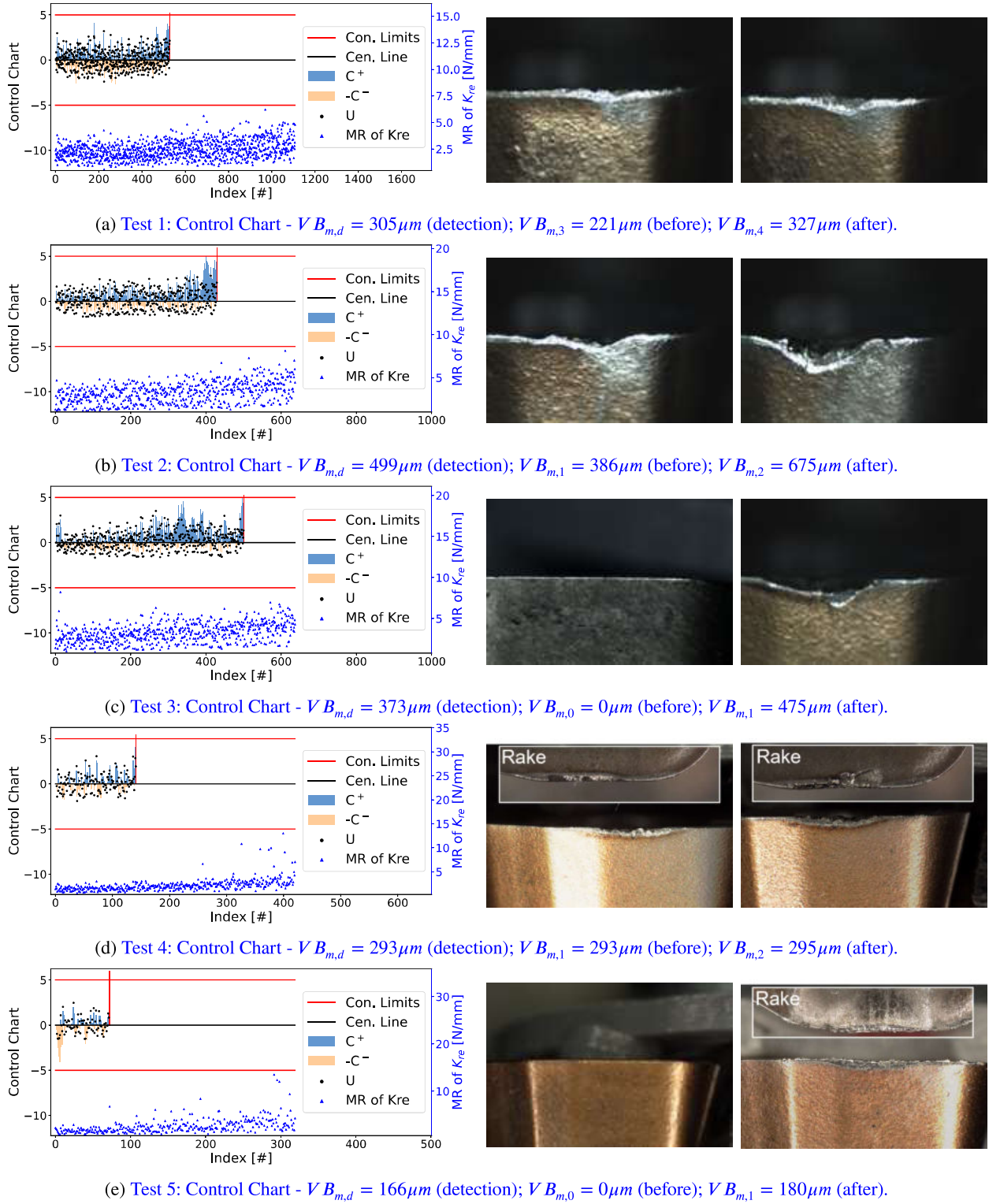


**Figure 7:** Control chart detections among the tests. Photos represent the tool wear at the stop before (middle) and after (right) the control chart detection.

#### 4.4. The influence of cutting conditions

The algorithm detects an out of control cutting process when the chipping phenomenon takes place on the rake face. The difference between the first three tests and the last two seems to be correlated to the adopted cutting speeds. Low speed machining brings to more intensive adhesion phenomena (Albertelli, Mussi, Strano and Monno (2021)), favouring notch wear occurrence. Furthermore, a difference between the two lubrication conditions was found at these cutting speeds. Cryogenic lubrication brought workpiece material to attach to the cutting edge (built-up-edge) on the cutting insert. Conversely, the cutting edge of conventional cooling at low speeds seemed cleaner, despite presenting notch wear, too. At high cutting speeds ( $125\text{m/min}$ ) the differences in the behaviour of the two lubrication conditions was less visible, bringing to small distributed chippings along the cutting edges. Despite these different phenomenological behaviours, the conceived algorithm behaved properly and was able to detect critical tool failures.

#### 4.5. Maximum flank wear measurements and sensitivity analysis

In figure 7, control charts were accompanied by the measured flank wears at the detection instants reported in the captions. It must be highlighted that flank wear measurements do not participate at all in the tool monitoring strategy. By the way, flank wear measurements were reported in order to contextualize the results of the proposed monitoring tool and to analyse from all the perspectives the out of control detections. The flank wear was computed making reference to the approaches explained in Albertelli et al. (2021); Albertelli, Mussi and Monno (2022) and standard ISO 3685 (ISO (1993)). Thus, for the cutter  $i$  at the  $k$ -th stop, a set of  $N_f$  local measurements of the flank width, indicated as  $VB_{ik,f}$ , was available. The maximum flank width of the  $i$ -th cutter at the  $k$ -th stop is indicated as  $VB_{m,ik}$  and is computed through eq. (40):

$$VB_{m,ik} = \max_{f \in [1, N_f]} VB_{ik,f} \quad (40)$$

Then, the maximum flank wear between the cutting inserts at the  $k$ -th stop is computed and reported as  $VB_{m,k}$  (eq. (41)):

$$VB_{m,k} = \max_{i \in [1, N]} VB_{m,ik} \quad (41)$$

The maximum flank wear values at the stop before and after the detection point (in figure 7 reported as  $VB_{m,k}$  and  $VB_{m,k+1}$ , with  $k$  assuming the corresponding stop number) are linearly interpolated to obtain maximum flank wear at the detection point (reported as  $VB_{m,d}$ ). Thus, the detection point  $d$  falls between stops  $k$  and  $k + 1$ . Let's call the observation numbers of these three points  $n_d$ ,  $n_k$  and  $n_{k+1}$ , respectively. Maximum flank wear in correspondence of the detection point  $VB_{m,d}$  is computed as follows (eq. (42)):

$$VB_{m,d} = VB_{m,k} + \frac{VB_{m,k+1} - VB_{m,k}}{n_{k+1} - n_k} (n_d - n_k) \quad (42)$$

In order to properly discuss the out of control detections, a sensitivity analysis of the algorithm was performed with respect to the control charts threshold. The results of such analysis were summarized in table 3. The first column of the table represents the case where  $H = 5\sigma_0$ . Such value is the standard one for a control chart of this kind (Montgomery (2008)). Thus, these results are obtained without any kind of training procedure or supervision. The reference  $VB_m$  is  $600\mu\text{m}$ , which is the flank wear threshold at which the run-to-failures were physically stopped (in accordance with ISO 3685, ISO (1993), and Nouri et al. (2015)). The results are compared with the ones obtained by Nouri et al. in Nouri et al. (2015). Five steel cutting tests were considered by the authors of the work. In order to compare results between the two condition monitoring systems, the reference mean flank wear was set to  $300\mu\text{m}$ , which was the tool wear criterion set by the researchers in accordance with the standard. Their results are reported for completeness in the last column of table 3. As can be seen, the mean of the relative percentage error (RPE) of the proposed method is  $-45\%$  with respect to the reference threshold of  $600\mu\text{m}$ . This means that the conceived tool monitoring strategy is conservative with respect to the tool wear criterion suggested by the flank wear. Anyway, it is of primary importance to underline that, as presented in section 4.3, an out of control detection is corresponding to severe damages on the cutting tools (such as micro chippings, chippings and notches), which lead to more severe implications for workpiece quality and operator safety than progressive tool wear (Li et al. (2022)). This is a symptom of the higher order of information carried by the cutting force signals with respect to a single information provided by flank wear (You, Gao, Guo, Liu,

**Table 3**

Control chart threshold sensitivity analysis results. Mean, standard deviation and maximum of relative percentage errors (RPE) are computed with respect to a threshold of  $VB_m = 600\mu m$  (maximum is computed using the absolute value of RPE, but is reported with the sign in order to keep the underestimation/overestimation case). For Nouri et al. (Nouri et al. (2015)) cases, RPE is reported with reference to  $VB_{mean} = 300\mu m$ .

Test	$H = 5\sigma_0$ $VB_{m,d} [\mu m]$	$H = 4\sigma_0 (-20\%)$ $VB_{m,d} [\mu m]$	$H = 6.5\sigma_0 (+30\%)$ $VB_{m,d} [\mu m]$	$H = 7.5\sigma_0 (+50\%)$ $VB_{m,d} [\mu m]$	$H = 10\sigma_0 (+100\%)$ $VB_{m,d} [\mu m]$	Nouri $VB_{mean,d} [\mu m]$
1	305	121	308	308	331	130
2	499	472	501	544	552	198
3	373	244	412	414	426	103
4	293	293	293	293	294	116
5	166	16	166	166	166	104
RPE Mean [%]	-45	-62	-44	-43	-41	-57
St. Dev. [%]	20	29	21	24	24	13
Max [%]	-72	-97	-72	-72	-72	-66

Li and Li (2022)). Furthermore, particular attention must be given to test 5 (the test facing the maximum relative error of  $-72\%$ ). In fact, the flank wear measurement is really low ( $166\mu m$ ) compared to the reference threshold ( $600\mu m$ ). This behaviour must be contextualised in the challenging cutting conditions of the test: cryogenic lubrication (which is not uniform as a conventional lubrication) and really high cutting speed ( $125m/min$ ). These parameters led to the formation of micro chippings in the cutting edge. Moreover, it was found that cryogenic lubrication lowers the frictional effect on the cutting tool, justifying a low flank wear. Compared to Nouri et al. results, the proposed method is less conservative ( $-45\%$  with respect to  $-57\%$  mean RPE). The uniformity in the detection outputs is similar, by looking at the RPE standard deviations (20% and 13% in favor of Nouri et al. method). The higher variance can be explained on the basis of two reasons: Nouri et al. method is based on mean cutting forces (from which more stable SFC can be inferred) and a mean flank wear indicator (in opposition to the maximum flank wear of the proposed study). Anyway, their method can't be used in any context, since continuously variable feed per tooth must be adopted. Furthermore, it has to be noticed that the method is providing a relatively uniform indication of tool wear in an unsupervised way, while changing machine tools, cutting conditions, lubrication media and degradation phenomena. Nouri et al. lower variability reflects also in a lower maximum RPE of  $-66\%$ . Relaxing the hypothesis of a fully unsupervised monitoring tool, it is possible to change the threshold of the control chart. This assumption can be relaxed either in presence of a training dataset or as long as data from the operational field are collected. In these cases it would be possible to tune the control chart threshold. Thus, in table 3, a sensitivity analysis of the proposed method with respect to the threshold of the control chart is proposed. It is possible to notice that test 5 (the one that presented the maximum RPE) is always detected to be out of control at  $166\mu m$ . This is a symptom of the fact that a severe modification of the signals was recorded. By analysing figure 7e, it is possible to notice that when the detection occurred, an evident degradation of the mean moving range was triggered, justifying the results of the sensitivity analysis. Cryogenic lubrication introduced a more complex degradation phenomenon in the cutting tool, which was the formation and propagation of micro cracks and edge chippings (visible on the rake face of fig. 7e). This result is important since highlights the higher content of information carried by the cutting force signals. Furthermore, moving towards higher control chart thresholds allows to reduce how much the method is conservative (leading to lower mean RPE). This could be helpful in case of light machining operations, instead of hard-to-cut materials machining, such as  $Ti_6Al_4V$ .

## 5. Conclusion

In this paper, an unsupervised tool wear monitoring strategy was conceived and validated. The proposition of a high-feed mechanistic model, an instantaneous forces-based specific force coefficients (SFC) fitting procedure (following Farhadmanesh and Ahmadi (2021)) and a self-starting tabular cusum control chart to detect an out of control cutting process were the key aspects. The main results of this work included:

- a new analytical mechanistic model for double-phased high-feed mills. The model includes the description of variable and gradual engagement of these cutting tools inside the material, while providing a parametric description of their geometry. The new formulation allows to identify SFC, where generic milling models can't.



- an improvement of the SFC fitting procedure proposed by Nouri et al. (2015) and Farhadmanesh and Ahmadi (2021). It includes an instantaneous identification of SFC, removing the need for continuously variable feed per tooth during the cutting operation (Nouri et al. (2015)). A principal component regression (PCR) approach was used in order to reduce the variability in the estimated SFC, due to the multicollinearity phenomenon. Multicollinearity doesn't allow to distinguish between the effects of the regressors. Thus, a small change in the experimental data may cause the coefficients to change according to the so-called see-saw effect. PCR implementation was proven to be efficient in limiting the multicollinearity phenomenon and naturally highlighting the tool wear information carried by SFC.
- an improvement of the solution proposed by Nouri et al. (2015) in terms of potentialities. Indeed, the conceived approach can be used to monitor the SFC with any occurring engagement condition, not relying on continuously variable feed during the workpiece machining in order to fit SFC. SFC can in fact be estimated directly from a small package of instantaneous cutting forces.
- the robustness with respect to working conditions. The conceived approach demonstrated to be valid among different cutting speeds (and thus degradation rates), lubrication conditions (i.e. conventional cooling and cryogenic, and thus chip formation mechanisms and wear phenomena) and machine tools, representing solid bases for solution portability.
- the correlation of the detection of out of control cutting process with 3D wear zones (notch wear phenomena) and chippings of the cutting edges. Providing a reliable and consistent detection of critical wear phenomena. Thus, the proposed solution resulted in a prompt detection of these brittle degradation phenomena which were critical for the continuation of  $Ti_6Al_4V$  cutting (Zhang et al. (2023)).
- a complete unsupervised solution. The solution does not present any tuning or training procedure. The algorithm does not require any training datum in order to be fully operative. Control charts were implemented in a self-starting fashion and thresholds were chosen to be standard.
- relatively uniform prediction of gradual wear, indicated through maximum flank wear. The fully unsupervised monitoring strategy resulted in a flank wear mean relative prediction error of  $-45\%$  with respect to a threshold of  $600\mu m$  (run-to-failure end). The peak relative error reached  $-72\%$ . Reference literature approaches reached a mean and peak relative error of  $-57\%$  and  $-66\%$  (Nouri et al. (2015)), respectively. The proposed method resulted to be less conservative than literature approach, while showing a higher variance in the detection. This was justified by the challenging variable conditions (different machine tools, lubrication media and cutting speeds) and the use of instantaneous cutting forces instead of mean ones.
- a sensitivity analysis of the control chart threshold with respect to the maximum flank wear at the detection point was performed. This resulted in a mean relative prediction error of  $-62\%$  (when the threshold was reduced by the 20%, and of  $-41\%$  (when the threshold was increased by 100%). These results give indications about how the predictions vary by tuning the control chart threshold in a supervised environment (if data from the field are collected and used to train the algorithm). Thus, the algorithm can be chosen to be either less conservative or more.

Future works of the proposed method include the introduction of prognostics solutions to estimate the Remaining Useful Life of the cutting tool and the SFC estimation based on more affordable measures like spindle currents (less invasive for industrial scenarios). Furthermore, research should focus on the correlation between the SFC evolution and the quality of cut left on the material surface.

## Acknowledgments

The authors would like to thank all Jobs S.p.A. staff that collaborated to the research experimental campaign. Moreover, the authors would like to thank SIAD for the cryogenic set-up preparation and MMC Italia Srl (Mitsubishi Materials) for the cutting tools. The present research was developed in the framework of the *DIGIMAN* project, funded by *Asse 1 – Azione 1.2.2 POR-FESR 2014 – 2020 Emilia-Romagna*, and a PhD grant (*ID27 - "Prognostics and Health Management in Machine Tool and Manufacturing Industry"*) in *DGR 769-2018* funded by *Emilia-Romagna* region.

## Declarations

The authors declare that they have no known competing financial interests or personal relationships that could have appeared to influence the work reported in this paper.

## CRedit authorship contribution statement

**Luca Bernini:** Conceptualization, Methodology, Software, Validation, Formal Analysis, Investigation, Writing. **Paolo Albertelli:** Conceptualization, Methodology, Validation, Investigation, Resources, Supervision. **Michele Monno:** Supervision.

## References

- Albertelli, P., Goletti, M., Torta, M., Salehi, M., Monno, M., 2016. Model-based broadband estimation of cutting forces and tool vibration in milling through in-process indirect multiple-sensors measurements. *International Journal of Advanced Manufacturing Technology* 82, 779–796. doi:10.1007/s00170-015-7402-x.
- Albertelli, P., Mussi, V., Monno, M., 2022. Development of generalized tool life model for constant and variable speed turning. *The International Journal of Advanced Manufacturing Technology* 118, 1885–1901. URL: <https://doi.org/10.1007/s00170-021-08017-y>, doi:10.1007/s00170-021-08017-y.
- Albertelli, P., Mussi, V., Strano, M., Monno, M., 2021. Experimental investigation of the effects of cryogenic cooling on tool life in ti6al4v milling. *The International Journal of Advanced Manufacturing Technology* 117, 2149–2161. URL: <https://doi.org/10.1007/s00170-021-07161-9>, doi:10.1007/s00170-021-07161-9.
- Altintas, Y., 2012. *Manufacturing Automation: Metal Cutting Mechanics, Machine Tool Vibrations, and CNC Design*. 2 ed., Cambridge University Press, Cambridge. URL: <http://doi.org/10.1017/CB09780511843723>, doi:10.1017/CB09780511843723.
- Arrazola, P.J., Özel, T., Umbrello, D., Davies, M., Jawahir, I.S., 2013. Recent advances in modelling of metal machining processes. *CIRP Annals* 62, 695–718. URL: <https://www.sciencedirect.com/science/article/pii/S0007850613001960>, doi:10.1016/j.cirp.2013.05.006.
- Aslan, A., 2020. Optimization and analysis of process parameters for flank wear, cutting forces and vibration in turning of AISI 5140: A comprehensive study. *Measurement* 163, 107959. URL: <https://linkinghub.elsevier.com/retrieve/pii/S0263224120304978>, doi:10.1016/j.measurement.2020.107959.
- Baur, M., Albertelli, P., Monno, M., 2020. A review of prognostics and health management of machine tools. *The International Journal of Advanced Manufacturing Technology* 107, 2843–2863. URL: [10.1007/s00170-020-05202-3](https://doi.org/10.1007/s00170-020-05202-3), doi:10.1007/s00170-020-05202-3.
- Bernini, L., Waltz, D., Albertelli, P., Monno, M., 2021. A novel prognostics solution for machine tool sub-units: The hydraulic case. *Proceedings of the Institution of Mechanical Engineers, Part B: Journal of Engineering Manufacture* URL: <https://doi.org/10.1177/09544054211064682>, doi:10.1177/09544054211064682.
- Campatelli, G., Scippa, A., 2012. Prediction of milling cutting force coefficients for Aluminum 6082-T4. *Procedia CIRP* 1, 563–568. URL: <http://dx.doi.org/10.1016/j.procir.2012.04.100>, doi:10.1016/j.procir.2012.04.100.
- Cheng, M., Jiao, L., Shi, X., Wang, X., Yan, P., Li, Y., 2020. An intelligent prediction model of the tool wear based on machine learning in turning high strength steel. *Proceedings of the Institution of Mechanical Engineers, Part B: Journal of Engineering Manufacture* 234, 1580–1597. URL: <https://doi.org/10.1177/0954405420935787>, doi:10.1177/0954405420935787.
- Duplak, J., Hatala, M., Duplakova, D., Steranka, J., 2018. Comprehensive analysis and study of the machinability of a high strength aluminum alloy (EN AW-AlZn5.5MgCu) in the high-feed milling. *Advances in Production Engineering & Management* 13, 455–465. URL: [http://apem-journal.org/Archives/2018/Abstract-APEM13-4\\_455-465.html](http://apem-journal.org/Archives/2018/Abstract-APEM13-4_455-465.html), doi:10.14743/apem2018.4.303.
- Eisenhauer, J.G., 2003. Regression through the origin. *Teaching Statistics* 25, 76–80. URL: <https://onlinelibrary.wiley.com/doi/abs/10.1111/1467-9639.00136>, doi:https://doi.org/10.1111/1467-9639.00136, arXiv:https://onlinelibrary.wiley.com/doi/pdf/10.1111/1467-9639.00136.
- Fang, N., Jawahir, I.S., Oxley, P.L., 2001. Universal slip-line model with non-unique solutions for machining with curled chip formation and a restricted contact tool. *International Journal of Mechanical Sciences* 43, 557–580. URL: <https://www.sciencedirect.com/science/article/pii/S0020740399001174>, doi:10.1016/S0020-7403(99)00117-4.
- Farhadmanesh, M., Ahmadi, K., 2021. Online identification of mechanistic milling force models. *Mechanical Systems and Signal Processing* 149, 1–18. URL: <https://doi.org/10.1016/j.ymssp.2020.107318>, doi:10.1016/j.ymssp.2020.107318.
- Guo, B., Zhang, Q., Peng, Q., Zhuang, J., Wu, F., Zhang, Q., 2022. Tool health monitoring and prediction via attention-based encoder-decoder with a multi-step mechanism. *The International Journal of Advanced Manufacturing Technology* URL: <https://link.springer.com/10.1007/s00170-022-09894-7>, doi:10.1007/s00170-022-09894-7.
- Guo, M., Wei, Z., Wang, M., Li, S., Liu, S., 2018. An identification model of cutting force coefficients for five-axis ball-end milling. *International Journal of Advanced Manufacturing Technology* 99, 937–949. URL: <https://doi.org/10.1007/s00170-018-2451-6>, doi:10.1007/s00170-018-2451-6.
- Hastie, T., Tibshirani, R., Friedman, J., 2009. *The Elements of Statistical Learning: Data Mining, Inference, and Prediction*. Second ed., Springer, New York. URL: <https://doi.org/10.1007/978-0-387-84858-7>, doi:10.1007/978-0-387-84858-7.
- Hintze, J.L., 2007. *NCSS: User's Guide III. Regression and Curve Fitting*. URL: <https://www.ncss.com/wp-content/uploads/2012/09/NCSSUG3.pdf>.
- ISO, 1993. ISO 3685: tool-life testing with single-point turning tools. ISO.

- Jiménez, A., Arizmendi, M., Sánchez, J.M., 2021. Extraction of tool wear indicators in peck-drilling of Inconel 718. *International Journal of Advanced Manufacturing Technology* 114, 2711–2720. URL: <https://link.springer.com/article/10.1007/s00170-021-07058-7>, doi:10.1007/S00170-021-07058-7/TABLES/4.
- Jozic, S., Lela, B., Bajić, D., 2014. A new mathematical model for flank wear prediction using functional data analysis methodology. *Advances in Materials Science and Engineering* 2014. doi:10.1155/2014/138168.
- Kumanchik, L.M., Schmitz, T.L., 2007. Improved analytical chip thickness model for milling. *Precision Engineering* 31, 317–324. URL: <http://dx.doi.org/10.1016/j.precisioneng.2006.12.001>, doi:10.1016/j.precisioneng.2006.12.001.
- Kuntoğlu, M., Aslan, A., Pimenov, D.Y., Usca, U.A., Salur, E., Gupta, M.K., Mikolajczyk, T., Giasin, K., Kapłonek, W., Sharma, S., 2020a. A Review of Indirect Tool Condition Monitoring Systems and Decision-Making Methods in Turning: Critical Analysis and Trends. *Sensors* 21, 108. URL: <https://www.mdpi.com/1424-8220/21/1/108>, doi:10.3390/s21010108.
- Kuntoğlu, M., Aslan, A., Sağlam, H., Pimenov, D.Y., Giasin, K., Mikolajczyk, T., 2020b. Optimization and Analysis of Surface Roughness, Flank Wear and 5 Different Sensorial Data via Tool Condition Monitoring System in Turning of AISI 5140. *Sensors* 20, 4377. URL: <https://www.mdpi.com/1424-8220/20/16/4377>, doi:10.3390/s20164377.
- Kurada, S., Bradley, C., 1997. A review of machine vision sensors for tool condition monitoring. *Computers in Industry* 34, 55–72. doi:10.1016/S0166-3615(96)00075-9.
- Letot, C., Serra, R., Dossevi, M., Dehombreux, P., 2015. Cutting tools reliability and residual life prediction from degradation indicators in turning process. *The International Journal of Advanced Manufacturing Technology* 86, 495–506. URL: <https://link.springer.com/article/10.1007/s00170-015-8158-z>, doi:10.1007/S00170-015-8158-z.
- Li, S., Zhu, K., 2021. In-situ tool wear area evaluation in micro milling with considering the influence of cutting force. *Mechanical Systems and Signal Processing* 161, 107971. URL: <https://linkinghub.elsevier.com/retrieve/pii/S0888327021003666>, doi:10.1016/j.ymssp.2021.107971.
- Li, X., Liu, X., Yue, C., Liang, S.Y., Wang, L., 2022. Systematic review on tool breakage monitoring techniques in machining operations. *International Journal of Machine Tools and Manufacture* 176, 103882. URL: <https://linkinghub.elsevier.com/retrieve/pii/S0890695522000335>, doi:10.1016/j.ijmachtools.2022.103882.
- Liu, D., Liu, Z., Zhao, J., Song, Q., Ren, X., Ma, H., 2022. Tool wear monitoring through online measured cutting force and cutting temperature during face milling Inconel 718. *The International Journal of Advanced Manufacturing Technology* URL: <https://link.springer.com/10.1007/s00170-022-09950-2>, doi:10.1007/s00170-022-09950-2.
- Matsumura, T., Tamura, S., 2017. Cutting force model in milling with cutter runout. *Procedia CIRP* 58, 566–571. URL: <http://dx.doi.org/10.1016/j.procir.2017.03.268>, doi:10.1016/j.procir.2017.03.268.
- Meng, X., Zhang, J., Xiao, G., Chen, Z., Yi, M., Xu, C., 2021. Tool wear prediction in milling based on a GSA-BP model with a multisensor fusion method. *International Journal of Advanced Manufacturing Technology* 114, 3793–3802. URL: <https://link.springer.com/article/10.1007/s00170-021-07152-w>, doi:10.1007/S00170-021-07152-W/TABLES/4.
- Montgomery, D.C., 2008. *Introduction to Statistical Quality Control*. Sixth ed., John Wiley & Sons, Inc.
- Montgomery, D.C., 2012. *Design and Analysis of Experiments*. Eighth ed., John Wiley & Sons, Inc.
- Nouri, M., Fussell, B.K., Ziniti, B.L., Linder, E., 2015. Real-time tool wear monitoring in milling using a cutting condition independent method. *International Journal of Machine Tools and Manufacture* 89, 1–13. URL: <https://doi.org/10.1016/j.ijmachtools.2014.10.011>, doi:10.1016/j.ijmachtools.2014.10.011.
- Pan, T., Zhang, J., Zhang, X., Zhao, W., Zhang, H., Lu, B., 2022. Milling force coefficients-based tool wear monitoring for variable parameter milling. *The International Journal of Advanced Manufacturing Technology* 120, 4565–4580. URL: <https://link.springer.com/10.1007/s00170-022-08823-y>, doi:10.1007/s00170-022-08823-y.
- Peng, Y., Dong, M., Zuo, M.J., 2010. Current status of machine prognostics in condition-based maintenance: a review. *The International Journal of Advanced Manufacturing Technology* 50, 297–313. URL: <https://doi.org/10.1007/s00170-009-2482-0>, doi:10.1007/s00170-009-2482-0.
- Stavropoulos, P., Papacharalampopoulos, A., Vasiliadis, E., Chrysosolouris, G., 2016. Tool wear predictability estimation in milling based on multi-sensorial data. *International Journal of Advanced Manufacturing Technology* 82, 509–521. doi:10.1007/s00170-015-7317-6.
- Wang, R., Song, Q., Liu, Z., Ma, H., Liu, Z., 2022. Multi-condition identification in milling Ti-6Al-4V thin-walled parts based on sensor fusion. *Mechanical Systems and Signal Processing* 164, 108264. URL: <https://linkinghub.elsevier.com/retrieve/pii/S0888327021006324>, doi:10.1016/j.ymssp.2021.108264.
- Wickramarachchi, C.T., Rogers, T.J., McLeay, T.E., Leahy, W., Cross, E.J., 2022. Online damage detection of cutting tools using Dirichlet process mixture models. *Mechanical Systems and Signal Processing* 180, 109434. URL: <https://linkinghub.elsevier.com/retrieve/pii/S0888327022005520>, doi:10.1016/j.ymssp.2022.109434.
- You, Z., Gao, H., Guo, L., Liu, Y., Li, J., Li, C., 2022. Machine vision based adaptive online condition monitoring for milling cutter under spindle rotation. *Mechanical Systems and Signal Processing* 171, 108904. URL: <https://linkinghub.elsevier.com/retrieve/pii/S0888327022000917>, doi:10.1016/j.ymssp.2022.108904.
- Zhang, P., Gao, D., Lu, Y., Wang, F., Liao, Z., 2022a. A novel smart toolholder with embedded force sensors for milling operations. *Mechanical Systems and Signal Processing* 175, 109130. URL: <https://linkinghub.elsevier.com/retrieve/pii/S0888327022002928>, doi:10.1016/j.ymssp.2022.109130.
- Zhang, X., Gao, Y., Guo, Z., Zhang, W., Yin, J., Zhao, W., 2023. Physical model-based tool wear and breakage monitoring in milling process. *Mechanical Systems and Signal Processing* 184, 109641. URL: <https://linkinghub.elsevier.com/retrieve/pii/S0888327022007270>, doi:10.1016/j.ymssp.2022.109641.
- Zhang, X., Pan, T., Ma, A., Zhao, W., 2022b. High efficiency orientated milling parameter optimization with tool wear monitoring in roughing operation. *Mechanical Systems and Signal Processing* 165, 108394. URL: <https://linkinghub.elsevier.com/retrieve/pii/S0888327021007469>, doi:10.1016/j.ymssp.2021.108394.

- Zhang, X., Wang, S., Li, W., Lu, X., 2021. Heterogeneous sensors-based feature optimisation and deep learning for tool wear prediction. *International Journal of Advanced Manufacturing Technology* 114, 2651–2675. URL: <https://link.springer.com/article/10.1007/s00170-021-07021-6>, doi:10.1007/S00170-021-07021-6/FIGURES/22.
- Zhang, X., Yu, T., Xu, P., Zhao, J., 2022c. In-process stochastic tool wear identification and its application to the improved cutting force modeling of micro milling. *Mechanical Systems and Signal Processing* 164, 108233. URL: <https://linkinghub.elsevier.com/retrieve/pii/S0888327021006051>, doi:10.1016/j.ymssp.2021.108233.
- Zhou, C., Guo, K., Sun, J., 2021. Sound singularity analysis for milling tool condition monitoring towards sustainable manufacturing. *Mechanical Systems and Signal Processing* 157, 107738. URL: <https://linkinghub.elsevier.com/retrieve/pii/S0888327021001333>, doi:10.1016/j.ymssp.2021.107738.
- Zhu, K., Yu, X., 2017. The monitoring of micro milling tool wear conditions by wear area estimation. *Mechanical Systems and Signal Processing* 93, 80–91. URL: <https://linkinghub.elsevier.com/retrieve/pii/S0888327017300687>, doi:10.1016/j.ymssp.2017.02.004.
- Zhu, K., Zhang, Y., 2019. A generic tool wear model and its application to force modeling and wear monitoring in high speed milling. *Mechanical Systems and Signal Processing* 115, 147–161. URL: <https://linkinghub.elsevier.com/retrieve/pii/S0888327018303042>, doi:10.1016/j.ymssp.2018.05.045.